

Morphologies of Reactive Nanolayer Stacks Sputtered on Ceramic Low-Temperature Cofired Ceramic Substrates Having a Micrometer-Scale Surface Roughness

Erik Wiss,* Alexander Schulz, Andreas Ruh, Konrad Jaekel, Jens Müller, and Steffen Wiese

The deposition of reactive multilayer systems (RMSs) is investigated on low-temperature cofired ceramic (LTCC) substrates having different surface morphologies. In this study, the morphologies of RMS layers that are deposited on glass-ceramic LTCC substrates are analyzed. Different surface morphologies are prepared through pretreatments of the LTCC surface. The considered surfaces encompass an untreated natural LTCC surface, a modified sintered LTCC surface by laser ablation, a surface with a deposited metallization layer, and finally, a surface with an additional solder layer put on the deposited metallization layer. The different pretreatments lead to significant differences in the roughness of the LTCC substrates, resulting in different reaction velocities and peak temperatures on the various surface morphologies after the RMS's reaction. As a result, different grades of structural integrity (liftoff, crack formation) between the reacted RMS layer and the LTCC are observed.

also be critical for sensitive components. To reduce the peak temperature and the total thermal budget for the global interconnection process, various approaches attempt to use localized heat sources from an exothermic reaction of a reactive compound deposit.^[1–11]

These reactive compounds or reactive multilayer systems (RMSs) consist of two or more reactant partners, which are arranged in alternating nanolayers in the range of 10–300 nm with a total stack thickness of up to 300 μm .^[12,13] A new intermetallic phase is built through intermixing on atomic level, if a sufficient amount of energy is applied (e.g., by a laser pulse, an electrical spark, or high temperature). During this exothermic process, a large amount of heat is released while the reaction front moves through the materials in the lateral direction.^[14]

If the amount of heat that was generated this way is higher than that removed by thermal diffusion, the exothermic reaction is termed self-propagating and keeps moving along the area of the RMS.^[15] Properties like generated heat, peak temperature, and reaction speed can be modified by changing the material combination, the ratio of the layer thicknesses, and the total thickness of the RMS stack. In addition to the Al–Ni system, which was used in this work, there are many other possible material combinations that can be used for RMS like Ti–Al, Nb–Si, or Pd–Al for example.^[16–18]

Whereas most of the RMS-related research focuses on silicon/silicon, metal/metal, or metal/silicon assemblies like die bonding or heat spreader mounting, there is a very limited amount of studies in other areas, which includes low-temperature cofired ceramics (LTCC).^[19–21] The use of RMS in the world of LTCC substrates would open another promising technological pathway, especially for heterogeneous assembly, but the properties of the ceramics affect the exothermic reaction. Compared to other materials like metal and silicon, the LTCC shows a higher surface roughness and a significantly lower thermal conductivity, which makes it very challenging to adapt the current knowledge to this technology.^[19,20] Therefore, further investigation is necessary to accomplish optimal circumstances for the deposition process of the RMS and hence the reaction itself.


The higher roughness of the LTCC substrate has a particular importance for any reactive joining technology. One aspect is the

1. Introduction

All established interconnection technologies in microelectronics (except ultrasonic wedge–wedge bonding and UV curing) are based on the transfer of heat into the joining zone. When heat is put in from the external sources, severe thermomechanical stresses can be induced into the assembly because of significant differences in the coefficients of thermal expansion (CTEs) between the component and the substrate materials. Heat might

E. Wiss, A. Ruh, S. Wiese
Chair of Microintegration and Reliability
Saarland University
66123 Saarbruecken, Germany
E-mail: erik.wiss@uni-saarland.de

A. Schulz, K. Jaekel, J. Müller
Department of Electronics Technology
Faculty of Electrical Engineering and Information Technology
TU Ilmenau
98693 Ilmenau, Germany

 The ORCID identification number(s) for the author(s) of this article can be found under <https://doi.org/10.1002/adem.202302284>.

© 2024 The Author(s). Advanced Engineering Materials published by Wiley-VCH GmbH. This is an open access article under the terms of the Creative Commons Attribution License, which permits use, distribution and reproduction in any medium, provided the original work is properly cited.

DOI: 10.1002/adem.202302284

compatibility with the deposition processes which are used to create a reactive multilayer on top of the surface. Some of these deposition processes, such as electrochemical deposition, demand a very even and smooth surface to deposit a stack of alternating thin layers with well-controlled thicknesses.^[6]

Another aspect is the mechanical strength of the bonded or soldered joints, which benefits from a high surface area (e.g., roughness or surface modification of the bonding partners), resulting in high mechanical interlocking between the component surface and the bonding agent.^[21–23]

Considering aspects of the joining process itself, the morphology of the component surface has a strong influence on the wetting behavior. In addition, the roughness of a ceramic substrate has an impact on the adhesion strength of applied thick films by influencing the mechanical interlocking. Thin films coated on a surface with a specific roughness show a similar surface morphology as the original surface.

To be able to address the question how the surface roughness or morphology alters the reaction of the RMS, the aim of the study was to manufacture-specified surface morphologies on glass-ceramic substrates. Therefore, different technologies which could provide surface morphologies in different scales had to be investigated. While an untreated LTCC substrate was used as a reference material, the surface of the other samples was modified using laser ablation to increase their roughness. In addition to this first surface treatment, a metallization layer using AgPd paste was screen-printed on the LTCC substrate before the RMS was deposited. Another variation consists of the deposition of a solder layer (Sn) on top of the screen-printed metallization before and after the deposition of the RMS.

2. Experimental Section

2.1. LTCC Substrates

To investigate the effects of different surface modifications of LTCC substrates on the deposition of reactive multilayers, various samples were produced and prepared in four different configurations. **Table 1** shows an overview in terms of the use of laser ablation and which type of metallization and solder coating was used, if any.

A commercially available DuPont GreenTape 951 was used for manufacturing the LTCC substrates under standard LTCC processing conditions, resulting in a total thickness of 840 μm after sintering. One of the substrates was used as reference material (configuration 1) without further processing, whereas the surface of the sample of configuration 2 was laser ablated to achieve higher roughness. For configuration 3, an AgPd metallization with a thickness of 5 μm was screen-printed on the LTCC

Table 1. Overview about the investigated samples.

Configuration	Laser ablation	Metallization	Solder coating
1	No	No	No
2	Yes	No	No
3	Yes	AgPd	No
4	Yes	AgPd	Yes

substrate using a DuPont 6146 paste before laser ablation. Configuration 4 was prepared in the same way, but an additional Sn-based solder coating of 2 μm was applied before and after the RMS was deposited to promote bonding adhesion to metal surfaces. After finishing all preparation steps, the samples were cut in smaller pieces of 15 mm \times 7 mm out of larger sheets by wafer sawing.

2.2. Laser Ablation

The AgPd-based metallization, which was screen-printed on the surface of the samples, was modified using laser ablation to achieve higher roughness on the metallization compared to the reference sample. The objective of this modification was the enhancement of the adhesion of the sputtered RMS layer. Modifying the surface in this way proved to be a good possibility due to its high precision and repeatability.^[24] Therefore, a 355 nm picosecond UV laser system microSTRUCT C v2.0 (3D-Micromac AG) was used. It provided a small laser spot diameter of 7 μm , very short laser pulses in a time range less than 10 ps, and a high laser pulse energy of up to 70 μJ , so that the heat-affected zone around the target was as small as possible. In this work, the laser power varied between 0.5 W (with metallization) and 0.8 W (without metallization), and the distance between two laser cutting lines was 40 μm with two repetitions.

2.3. Surface Characterization

Before the RMS was deposited, the surface of both the modified and the unmodified LTCC surfaces was measured using a laser scanning microscope (LSM) Olympus LEXT OLS4100 (Olympus Europa SE & Co. KG) with a 50 \times objective and a numerical aperture of 0.95. Therefore, the surface was scanned in smaller areas of 250 μm \times 250 μm . The values used in this work are the core height S_k , the reduced peak height S_{pk} , the reduced dale height S_{vk} , and the material ratios S_{mr1} and S_{mr2} , which are presented in Abbott–Firestone curves.

2.4. Deposition of RMS and Solder Layer

The deposition of the RMS on all the differently prepared LTCC substrates as well as the deposition of the solder layer for configuration 4 were realized by a sputter process using a PVD system CS400 (VON ARDENNE GmbH) whose working principle is predicated on magnetron deposition. In case of configuration 4, a thin layer of 2 μm tin was sputtered first on the metallization. After that — and in every other case — the RMS itself was deposited, consisting of alternating layers of aluminum and nickel. To achieve the maximum heat release during the exothermic reaction layer, thicknesses of 60 nm for aluminum and 40 nm for nickel, corresponding to a stoichiometry ratio of 3:2, were chosen with 100 bilayers leading to a total thickness of 10 μm for the RMS. Again, only the samples of configuration 4 were covered with 2 μm tin.

2.5. Scanning Electron Microscopy Analysis

The cross sections of the samples were prepared for scanning electron microscopy (SEM) using a ZEISS EVO MA15 (Carl

Zeiss Microscopy). The targeted magnification was in the range between $2000\times$ and $80\,000\times$. Therefore, samples were prepared in a specific manner using the following sequence of five preparation steps. Step 1: after embedding with Struers EpoFix kit, the samples were cut using an IsoMet 4000 precision saw (Buehler). Step 2: grinding of metallographic samples was carried out on SiC foils with grits of 500 and 1200 on a LabPol-25 (Struers). Step 3: the first polishing steps were carried out on a Tegramin-25 (Struers) by using various diamond suspensions having 9, 3, and $1\ \mu\text{m}$ particle sizes. Step 4: the final polishing was performed on an ATM Saphir Vibro vibratory polishing machine using a colloidal silicon oxide. This resulted in an extremely even surface with ultralow roughness which enables to resolve the RMS nanolayers in the later SEM. Step 5: the sample coating was carried out on a Q150T Coater (Quantum Design). A very thin carbon film was sputtered on the sample to retain the even surface of the final polishing step. The target thickness of the carbon film was 20 nm. The ZEISS EVO was configured with a LaB_6 cathode, 20 kV accelerating voltage, and a beam current of $40\ \mu\text{A}$ to carry out the respective microscopy.

2.6. Determination of Reaction Front Velocity and Peak Temperature

To achieve information about the speed and temperature of the reaction, corresponding measurements were performed. Therefore, a high-speed pyrometer KGA Series 840 (KLEIBER Infrared GmbH) with a measurement time of $10\ \mu\text{s}$ and a high-speed camera Fastcam SA-X2 type 480 K (Photron Deutschland GmbH) with a Navitar 12x zoom lens were used. The RMSs were ignited electrically by connecting two test probes to a power supply (25 V, 4 A), that were shorted by a section of the RMS.

3. Results

3.1. Raw Unmachined LTCC

The cross section of a sample without further processing is shown in **Figure 1** (remark: the gap between the RMS and the

LTCC in **Figure 1a** is supposed to be caused by the mechanical preparation of the sample). The reactive Al–Ni multilayer (narrow light gray stripe on top) was directly deposited on the raw unmachined LTCC substrate (mixed gray area). Due to the higher roughness of the ceramic compared to silicon or metal substrates, the deposited RMS follows the surface and looks wavy, but still continuous without any interruptions. In the 15 000-times magnified **Figure 1b** of the RMS, the single nanolayers can be seen.

3.2. Laser-Ablated LTCC

The cross section of a sample, which was laser ablated before the RMS was deposited, can be seen in **Figure 2**. The RMS changed from a wavy look with continuous layers to a stack consisting of many separated columns, whose sidewalls are not fully connected. The locations, which were engraved by the laser, experienced a material deposition leading to a height difference in the surface. Due to this difference, it is not possible to form a continuous layer anymore, although the deposition still reaches the bottom of the LTCC substrate.

3.3. Laser-Ablated LTCC with Metallization Layer

The laser-ablated samples with the AgPd metallization show the same behavior as the laser-ablated samples without metallization regarding the formation of separated columns. Adding this layer results in a surface, which is more rugged than in the other cases (see **Figure 3**). This effect is even more visible when solder layers are used (see **Figure 4**; remark: the round whitish particles with a diameter of $\approx 100\ \text{nm}$ in **Figure 3b** and **4b** are only a side effect of the sputter-coating preparation).

3.4. LSM Measurements

The LSM measurements of all configurations are depicted as Abbott–Firestone curves that are aligned to the average height. The used parameters are the core height S_k , the reduced peak height S_{pk} , the reduced dale height S_{vk} , and the material ratios S_{mr1} and S_{mr2} , which can be found in **Table 2**.

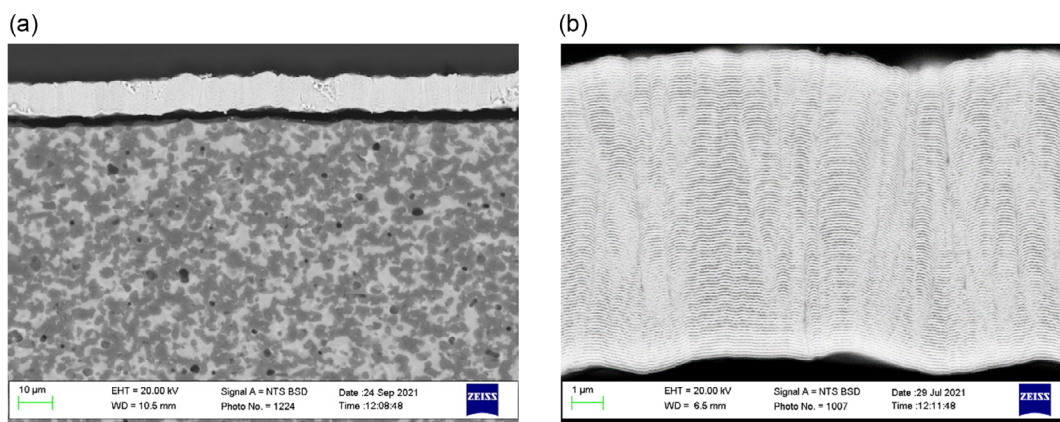


Figure 1. SEM images of the sputtered RMS (light gray) on an unmachined LTCC substrate (mixed gray). The RMS seems to be very smooth with nearly no interruptions. Magnification: a) $2000\times$ and b) $15\,000\times$.

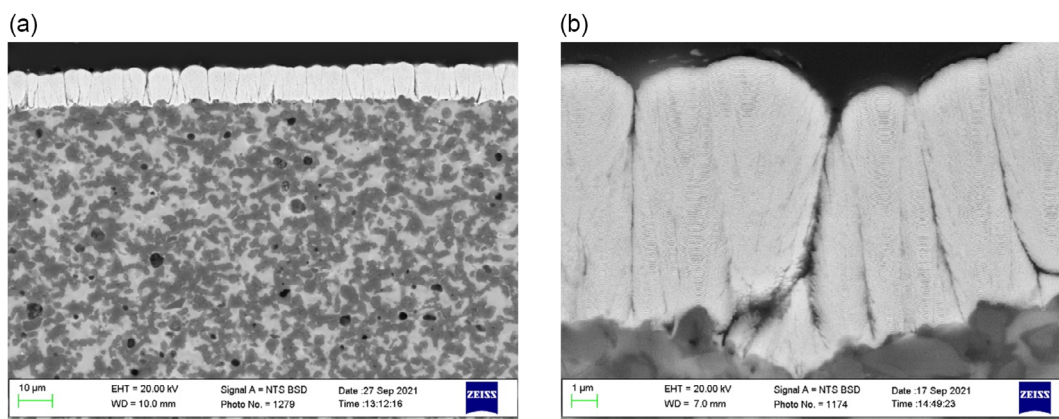


Figure 2. SEM images of the sputtered RMS (light gray) on a laser-ablated LTCC substrate (mixed gray). The RMS seems to be rugged with a lot of interruptions and separated columns whose sidewalls are not fully connected. Magnification: a) 2000 \times and b) 15 000 \times .

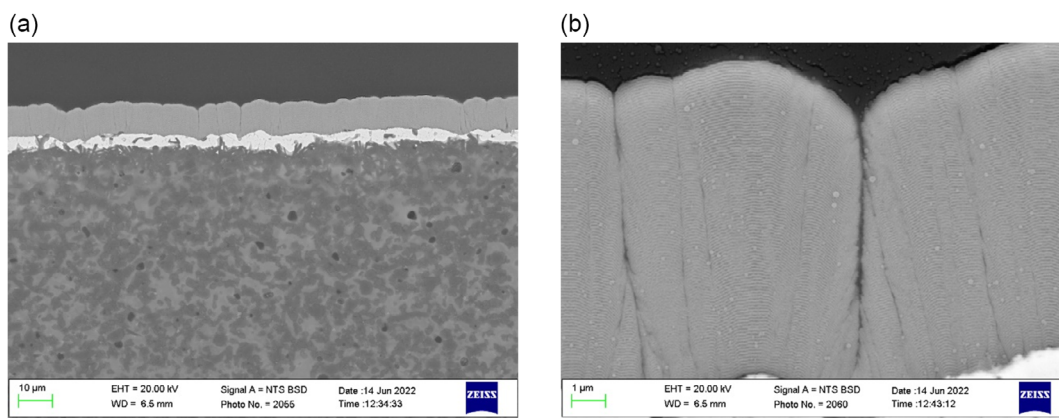


Figure 3. SEM images of the sputtered RMS (dark gray) on a laser-ablated LTCC substrate (mixed gray) with AgPd metallization (light gray). The metallization transmits the rugged surface of the LTCC to the RMS, which forms separated columns. Magnification: a) 2000 \times and b) 20 000 \times .

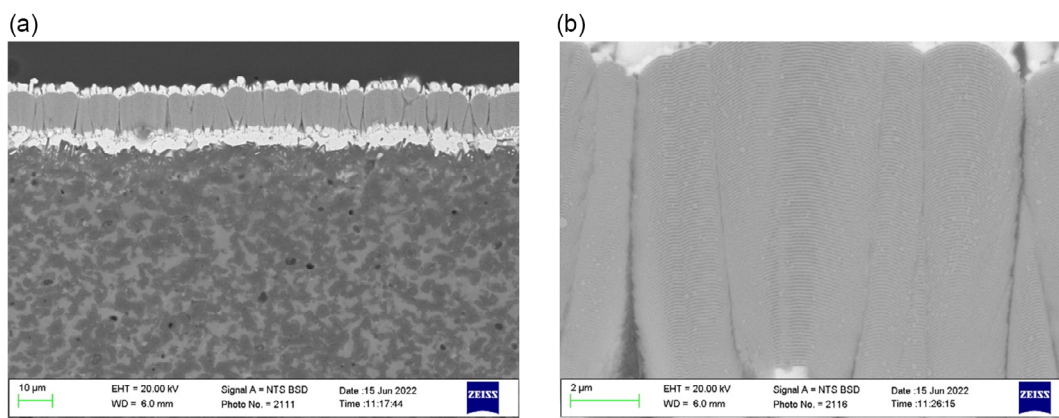


Figure 4. SEM images of the sputtered RMS (dark gray) on a laser-ablated LTCC substrate (mixed gray) with AgPd metallization and solder layers (light gray). Both the metallization and the solder layer transmit the rugged surface of the LTCC to the RMS. Magnification: a) 2000 \times and b) 20 000 \times .

Table 2. Results of the LSM measurements: core height S_k , reduced peak height S_{pk} , reduced dale height S_{vk} , and material ratios S_{mr1} and S_{mr2} .

Configuration	Core height S_k [μm]	Reduced peak height S_{pk} [μm]	Reduced dale height S_{vk} [μm]	Material ratio S_{mr1} [%]	Material ratio S_{mr2} [%]
1	1.4097	0.6138	0.5187	9.69	89.85
2	1.9667	0.8175	0.6621	10.82	91.67
3	2.8483	1.1915	1.0783	9.02	89.75
4	2.9521	1.5055	1.0375	10.09	90.61

The calculated values are in good agreement with the SEM images of the cross sections: the core height of the unmachined LTCC sample has the lowest value of 1.41 μm , followed by 1.97 μm for the laser-ablated samples, and 2.85 μm and

2.95 μm for the samples with metallization, both with and without solder layers, respectively.

Figure 5 shows the effect of the laser ablation on the morphology. Whereas the distribution of the core height is relatively small in case of the unmachined LTCC sample, there is a small widening after modifying the surface. The core height increases by $\approx 0.56 \mu\text{m}$, and the reduced peak and dale height increase by $\approx 0.14\text{--}0.2 \mu\text{m}$.

Adding an AgPd metallization layer results in a greater widening of the height distribution as before (see **Figure 6**) and in an increase of the measured values (core height of 2.85 μm , reduced peak height of 1.19 μm , and reduced dale height of 1.1 μm), what indicates a more rugged surface. The effect is even more visible when the metallization layer is combined with additional solder layers (core height of 2.95 μm , reduced peak height of 1.51 μm , and reduced dale height of 1.04 μm).

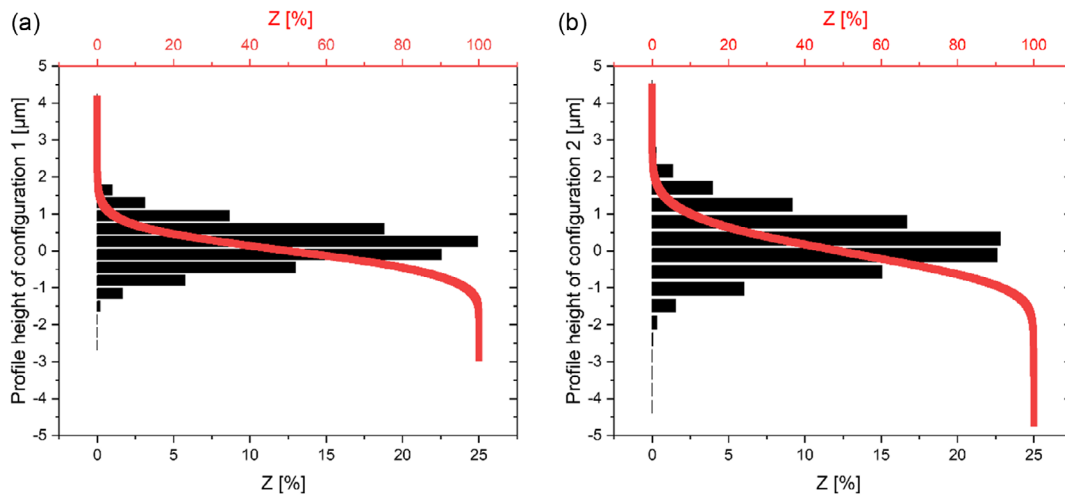


Figure 5. Abbott–Firestone curves of a) configuration 1 (raw unmachined reference material) and b) configuration 2 (laser-ablated LTCC). The laser ablation of the LTCC surface results in a small widening of the height distribution.

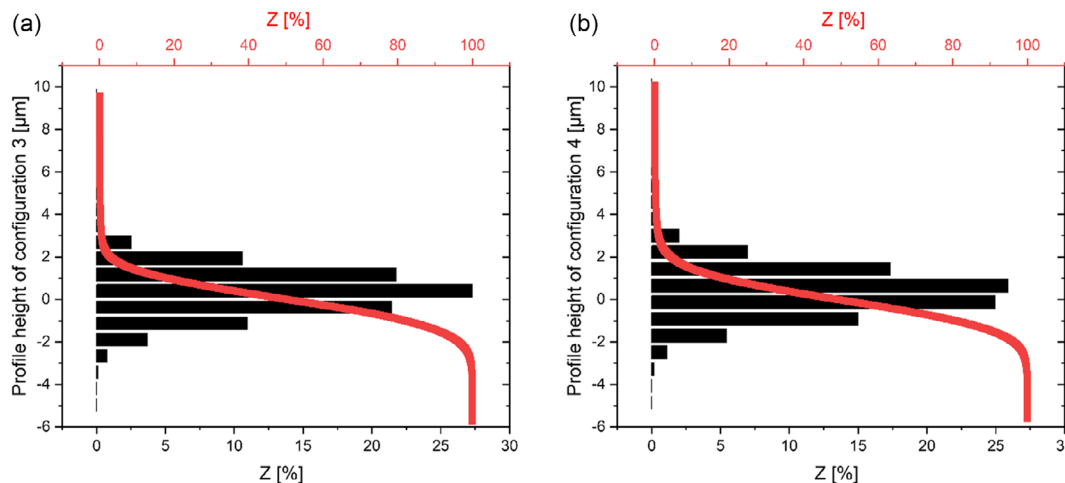


Figure 6. Abbott–Firestone curves of a) configuration 3 (laser-ablated LTCC with AgPd metallization) and b) configuration 4 (laser-ablated LTCC with AgPd metallization and additional solder layers). Compared to the previous curves, the metallization seems to cause a greater widening of the height distribution.

3.5. Reaction Front Velocity and Peak Temperature

The velocity and temperature measurements of the reactive multilayers exothermic reaction are shown in **Table 3** and have been described in detail earlier.^[25,26] The unmodified LTCC substrate shows the highest peak temperature with almost 1100 °C and the highest reaction front velocity with 5.0 m s⁻¹. Modifying the surface by laser ablation and the use of a metallization layer decrease

Table 3. Results of the mean speed and maximum temperature measurements for the different configurations.^[25,26]

Configuration	Peak temperature [°C]	Reaction front velocity [m s ⁻¹]
1	1092	5.0
2	803	2.9
3	739	2.2
4	838	2.4

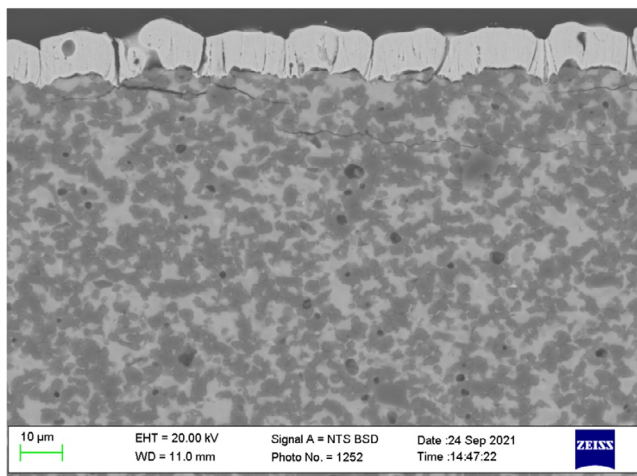


Figure 7. SEM image of a detached RMS (dark gray) from a laser-ablated LTCC substrate (mixed gray) with cracks in the ceramic after ignition. Magnification: 2000×.

these values, e.g., configuration 3 reached the lowest values with a peak temperature of only 739 °C and a reaction front velocity of 2.2 m s⁻¹. Adding the solder layers in configuration 3 results in a small increase in the measured values. The results of configurations 2–4 do not differ significantly, given the fact that the depositions of the respective RMS layers were not carried out in the same process. Therefore, it is very difficult to read a trend from the three latter results in Table 3.

Figure 7 shows the SEM image of a reacted RMS on a laser-ablated LTCC substrate. The RMS is detached from the surface over large areas and there are some cracks within the ceramic substrate due to the high temperature of the reaction, caused by the difference in the CTEs of the deposited RMS and the ceramic substrate. Local adhesion is reached where the laser engraved the surface.

A top view of a deposited RMS can be seen in **Figure 8a** while a reacted RMS is shown in **Figure 8b**. Several pores and microcracks have formed on the surface of the multilayer. Such pores could not be observed in reacted multilayers that were deposited and ignited on raw unmachined LTCC surfaces. The pores seem to support the adhesion between the multilayer and the LTCC substrate, and their formation seems to prevent major cracks within the layer due to a shrinkage in its volume during the exothermic reaction. In literature, a decrease in the volume of up to 12% is reported.^[27]

4. Discussion

The comparison of the four studied configurations with different surface modifications reveals significant differences in the appearance of the RMS, which can have several consequences for following joining processes.

In the case of the unmodified reference LTCC substrate, its morphology is transmitted to the deposited RMS, leading to a wavy surface and continuous layers without any interruptions although the roughness of the surface in the range of several hundred micrometers is much higher than that of silicon with less than 1 nm. From the ignition experiments, it can be deduced that this continuity lets the reaction progress at the highest speed of the four configurations, reaching the highest

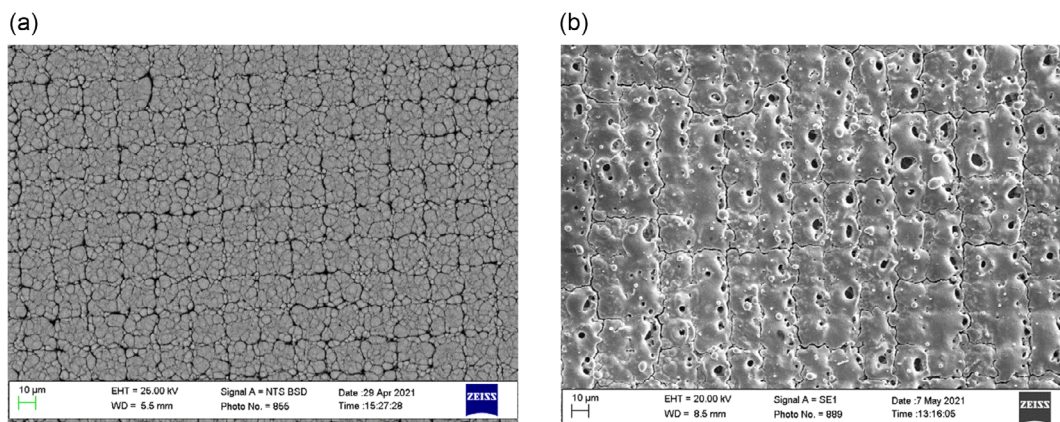


Figure 8. a) Top view of an RMS that was deposited on a laser-ablated LTCC surface. It can be seen where the laser engraved the ceramic. Magnification: 1000×. b) Top view of a reacted RMS with microcracks and pores within the surface of the RMS. Magnification: 1000×.

peak temperature of almost 1100 °C. One reason for this high temperature is the much lower thermal conductivity of the LTCC ($3.3 \text{ W m}^{-1} \text{ K}^{-1}$) compared to silicon ($152 \text{ W m}^{-1} \text{ K}^{-1}$) or silver ($429 \text{ W m}^{-1} \text{ K}^{-1}$), fortified by the observed liftoff of the RMS that removes the direct contact between the RMS and the substrate. It can be assumed that this liftoff is caused by the formation of huge thermomechanical stress within the material due to the very high temperature rise in a very short time period of a few milliseconds. Additionally, the volume of the RMS decreases during the exothermic reaction, which lowers the adhesion in combination with the mismatch in the CTEs of the different materials.

The adhesion can be increased by laser ablating the surface of the substrate. The local material removal at the processed areas results in the formation of trenches across the entire surface. If the RMS is deposited on a surface treated in this way, no continuous layers can be created due to the abrupt changes in height. The morphology of the nanolayers changes from a wavy look to a more rugged one, with a lot of interruptions resulting in the formation of separated columns that are not fully connected between their sidewalls. This has several consequences: first, at every interruption, the intermixing of the materials and, hence, the reaction front is stopped until the generated heat reactivates the process in the next section, which can be assumed to be the main factor for the observed decrease in the reaction speed. Furthermore, the same amount of heat as before is released in less time, resulting in a decrease in absolute temperature and thus, lowers thermomechanical stress. Second, the adhesion is improved due to the anchoring effect of the deposited RMS in the substrate. Third, the mechanical anchoring of the RMS in combination with the mismatch in the CTEs and the volume reductions leads to microcracks in the structure. Furthermore, less peeling effects could be observed.

As before, the usage of a laser-ablated metallization layer and, if applied, an additional solder layer leads to a rugged appearance in the RMS and the formation of unconnected columns. The velocity of the reaction and the temperature are reduced due to the same reasons as in the last configuration. The drop in temperature is higher because a part of the thermal energy is absorbed in the metallization. It is supposable that the solder layer can also be used to fill potential microcracks within the RMS, if enough pressure is used during the joining process.

5. Conclusions

The deposition of RMSs has been investigated on glass-ceramic LTCC substrates, having different surface morphologies. The results show that the deposition of an RMS on unmachined LTCC substrates results in uninterrupted layers with a very smooth and wavy appearance. This morphology of layers shows the highest peak temperature and highest velocity of the exothermic reaction and leads to a liftoff of the resulting intermetallic layer after the reaction. It is assumed that the high temperature gradients, which cause high thermomechanical stress, and the different CTEs are responsible for the liftoff. The usage of an additional metallization layer underneath RMS partly prevents the liftoff but creates cracks in the LTCC surface.

When the roughness of the ceramic substrate is increased by laser ablation, an improved local adhesion of the reacted multilayer can be observed. The deposited RMS appears as an interrupted layer with a column-like structure. Despite its non-continuous appearance, the reaction still propagates along the surface, but shows both a lower peak temperature and reaction velocity. Although a liftoff is prevented, cracks in the LTCC surface are observed after the reaction. The addition of a solder layer leads to a similar appearance of the deposited multilayer. However, no cracks are observed after the reaction.

It is believed that the low thermal conductance of the glass-ceramic LTCC substrate leads to higher temperature gradients compared to other substrate materials like Si or metal. Thus, higher thermomechanical stresses during the reaction may cause a liftoff of the reacted RMS layer. Increasing the LTCC surface roughness by laser ablation or deposition of metallization layers helps to increase the layer adhesion. The introduction of an intermediate solder layer seems to effectively reduce the thermomechanical stresses and prevents crack formation within the LTCC substrate.

Acknowledgements

This work was funded by the Deutsche Forschungsgemeinschaft (DFG, German Research Foundation) — Project ID 426204742 and funding codes BA 6161/1-1 and BA 6161/1-2.

Support in sample preparation (LTCC manufacturing, sputter processing) was received from Ms. Ina Koch and Mr. Joachim Döll from the Center of Micro- and Nanotechnologies (ZMN) (DFG resources reference: RI_00009), which runs DFG-funded core facilities (grant nos. MU 3171/2-1 + 6-1, SCHA 632/19-1 + 27-1, HO 2284/4-1 + 12-1) at TU Ilmenau.

Open Access funding enabled and organized by Projekt DEAL.

Conflict of Interest

The authors declare no conflict of interest.

Data Availability Statement

Research data are not shared.

Keywords

Al–Ni, joining, low-temperature cofired ceramics, reactive multilayers, reactive multilayer system

Received: December 31, 2023

Revised: May 1, 2024

Published online: May 29, 2024

- [1] J. Braeuer, T. Gessner, *J. Micromech. Microeng.* **2014**, *24*, 115002.
- [2] B. Boettge, J. Braeuer, M. Wiemer, M. Petzold, J. Bagdahn, T. Gessner, *J. Micromech. Microeng.* **2010**, *20*, 064018.
- [3] J. Braeuer, J. Besser, M. Wiemer, T. Gessner, *Sens. Actuator, A* **2012**, *188*, 212.
- [4] S. Kanetsuki, S. Miyake, K. Kuwahara, T. Namazu, *Jpn. J. Appl. Phys.* **2016**, *55*, 06GP17.

- [5] S. Kanetsuki, K. Kuwahara, S. Egawa, S. Miyake, T. Namazu, *Jpn. J. Appl. Phys.* **2017**, *55*, 06GN16.
- [6] S. Hertel, W. Schulte, M. Weiser, M. Becker, M. Wiemer, T. Otto, in *Micro-Nano-Integration; 7th GMM-Workshop (VDE)* **2018**, p. 1.
- [7] X. Qiu, *Master Thesis, Louisiana State University*, August **2007**.
- [8] J. Wang, E. Besnoin, A. Duckham, S. J. Spey, M. E. Reiss, O. M. Knio, M. Powers, M. Whitener, T. P. Weihs, *Appl. Phys. Lett.* **2003**, *83*, 3987.
- [9] J. Matteau, in *Proc. Int. Symp. Microelectron*, Long Beach, CA, October **2011**, Vol. 1, p. 000521.
- [10] J. S. Subramanian, P. Rodgers, J. Newson, T. Rude, Z. He, E. Besnoin, T. P. Weihs, V. Evely, M. Pecht, in *EuroSimE*, Berlin, Germany, April **2005**, p. 681.
- [11] A. P. McClure, *Master Thesis, University of Maryland*, October **2008**.
- [12] S. Sen, M. Lake, N. Kroppen, P. Farber, J. Wilden, P. Schaaf, *Appl. Surf. Sci.* **2017**, *396*, 1490.
- [13] D. P. Adams, *Thin Solid Films* **2015**, *576*, 98.
- [14] K. Raić, R. Rudolf, P. Ternik, Z. Žunič, V. Lazić, D. Stamenković, T. Tanasković, I. Anžel, *Mater. Tehnol.* **2011**, *45*, 335.
- [15] A. J. Gavens, D. Van Heerden, A. B. Mann, M. E. Reiss, T. P. Weihs, *J. Appl. Phys.* **2000**, *87*, 1255.
- [16] A. S. Rogachev, A. É. Grigoryan, E. V. Illarionova, I. G. Kanel', A. G. Merzhanov, A. N. Nosyrev, N. V. Sachkova, V. I. Khvesyuk, P. A. Tsygankov, *Combust., Explos. Shock Waves* **2004**, *40*, 166.
- [17] M. E. Reiss, C. M. Esber, D. Van Heerden, A. J. Gavens, M. E. Williams, T. P. Weihs, *Mater. Sci. Eng. A* **1999**, *261*, 217.
- [18] A. S. Ramos, M. T. Viera, *Intermetallics* **2012**, *25*, 70.
- [19] H. Jantunen, T. Kangasvieri, J. Vähäkangas, S. Leppävuori, *J. Eur. Ceram. Soc.* **2003**, *23*, 2541.
- [20] M. Matters-Kammerer, U. Mackens, K. Reimann, R. Pietig, D. Hennings, B. Schreinemacher, R. Mauczok, S. Gruhlke, C. Martiny, *Microelectron. Reliab.* **2006**, *46*, 134.
- [21] Satyanarayan, K. N. Prabhu, *J. Mater. Sci. Technol.* **2013**, *29*, 1430.
- [22] J. K. Shang, D. Yao, *J. Electron. Packag.* **1996**, *118*, 170.
- [23] B. Feng, J. Cao, Y. Wang, J. Feng, *ECSJ. Solid State Sci. Technol.* **2015**, *5*, P41.
- [24] N. Gutzeit, T. Welker, K. H. Drüe, J. Müller, in *Additional Papers and Presentations (CICMT)*, Denver, CO, April **2016**, Vol. 2016, p. 000103.
- [25] A. Schulz, H. Bartsch, N. Gutzeit, S. Matthes, M. Glaser, A. Ruh, J. Müller, P. Schaaf, J. P. Bergmann, S. Wiese, in *MikroSystemTechnik Congress (VDE)*, Ludwigsburg, Germany, November **2021**.
- [26] A. Schulz, A. Ruh, S. Wiese, J. Müller, in *Ceramic Interconnect and Ceramic Microsystems Technologies (CICMT)*, Vienna, Austria, July **2022**.
- [27] T. Namazu, K. Ohtani, K. Yoshiki, S. Inoue, in *16th Inter. Solid-State Sensors, Actuators and Microsystems Conf. (IEEE)*, IEEE, Beijing, China **2011**, p. 1368.